Environmental Pollution 389 (2026) 127434

Contents lists available at ScienceDirect

Environmental Pollution

journal homepage: www.elsevier.com/locate/envpol

Polypropylene nanoplastics as PFAS carriers: A computational study of the adsorption mechanism

Valentina Migliorati [a,*], Federica Simonetti [b], Luca Bertagnin [a], Enrico Bodo [a,*]

[a] Department of Chemistry, Sapienza University of Rome, P.le Aldo Moro 5, 00185, Rome, Italy
[b] Department of Science and Engineering of Matter, Environment and Urban Planning, Marche Polytechnic University, Via Brecce Bianche 12, 60131, Ancona, Italy

ARTICLE INFO

Keywords:
PFAS
Computational procedure
Nanoplastic
Drinking water
Adsorption mechanism

ABSTRACT

Polypropylene (PP) is a major constituent of nanoplastics (NPs) found worldwide in aquatic environments, where it promotes the co-transport of contaminants. Of particular concern is the co-transport of perfluoroalkyl substances (PFAS), potentially increasing the uptake and bioaccumulation of PFAS in organisms during simultaneous exposure. Since the adsorption mechanism of PFAS molecules on NPs is still only partially understood, we have carried out a thorough systematic investigation of how a range of PFAS interact with PP nanoplastics. To this end, we developed a computational procedure which combines molecular mechanics, semiempirical methods and density functional theory calculations. We were able to describe quantitatively the adsorption process, revealing similarities and differences in the adsorption behavior as a function of the PFAS length, branching and of the nature of the PFAS polar head. Our findings suggest that the nanoplastic possess a certain degree of local flexibility which allows it to effectively adsorb all the investigated compounds, by modifying its form to maximize the interactions with PFAS. The adsorption mechanism is mainly driven by dispersion forces between the PFAS perfluorinated chain and the nanoplastic polymeric chain, with minor electrostatic contributions. These findings represent a significant step forward in the rationalization of PFAS adsorption behavior, which is essential not only to clarify their environmental fate but also to help develop strategies for PFAS removal from contaminated water sources.

1. Introduction

Perfluoroalkyl substances (PFAS) represent a large group of man-made chemicals characterized by carbon chains bonded to fluorine atoms. PFAS contamination is becoming an increasingly serious issue, now recognized as a global environmental emergency due to their persistence, widespread presence, and harmful impact on ecosystems and human health (Cousins et al., 2022; Kurwadkar et al., 2022). PFAS are widely used in industrial and consumer products due to their ability to repel oil and water. However, many PFAS are extremely persistent, remaining in the environment for decades and accumulating in the human body with elimination half-lives that span several years. Recent EPA regulations targeting certain PFAS are based on extensive epidemiological and laboratory research linking them to cancer and other adverse health outcomes (Wee and Aris, 2023; Joo et al., 2021; Fenton et al., 2021; Wee and Aris, 2017; Podder et al., 2021; Deep and Ahluwalia, 2001). These findings have drawn significant media coverage, highlighting the risks associated with these so-called "forever chemicals", including their role as endocrine disruptors and their potential to contribute to a wide array of chronic health conditions, through mechanisms involving immune system interference, liver toxicity, disruption of cell membranes, and altered energy metabolism (Wee and Aris, 2023; Joo et al., 2021; Fenton et al., 2021; Wee and Aris, 2017; Podder et al., 2021; Deep and Ahluwalia, 2001).

The most widespread and concerning form of PFAS contamination affects water basins, which are increasingly polluted not only by these persistent chemicals but also by nanoplastics (NPs) (Sandoval et al., 2024; Pizzini et al., 2024; Hernando et al., 2006). With global plastic production continuing to rise steadily, reaching around 322 million tons in 2015, plastic pollution has indeed become one of the most significant threats to both marine life and human health (Brandts et al., 2018; Koelmans et al., 2019). NPs are typically formed through the degradation of older microplastics via sunlight exposure, industrial production, or the everyday use of consumer products ((Peng et al., 2020)) and their presence in water has been increasingly investigated due to their ability to remain highly stable and widely dispersed (Gigault et al., 2018; Bergmann et al., 2022; Enfrin et al., 2019; Pelegrini et al., 2023). NPs exhibit distinctive physicochemical characteristics at the nanoscale, enabling them to penetrate biological barriers, disrupt cellular functions, and accumulate within organisms (Yee et al., 2021; Llorca

* Corresponding authors.
E-mail addresses: valentina.migliorati@uniroma1.it (V. Migliorati), enrico.bodo@uniroma1.it (E. Bodo).

https://doi.org/10.1016/j.envpol.2025.127434
Received 23 July 2025; Received in revised form 10 November 2025; Accepted 22 November 2025
Available online 24 November 2025
0269-7491/© 2025 The Authors. Published by Elsevier Ltd. This is an open access article under the CC BY license (http://creativecommons.org/licenses/by/4.0/).

Fig. 1. Co-transport mechanism of PFAS by adsorption onto nanoplastics in water ecosystems and their biomagnification through the food chain.

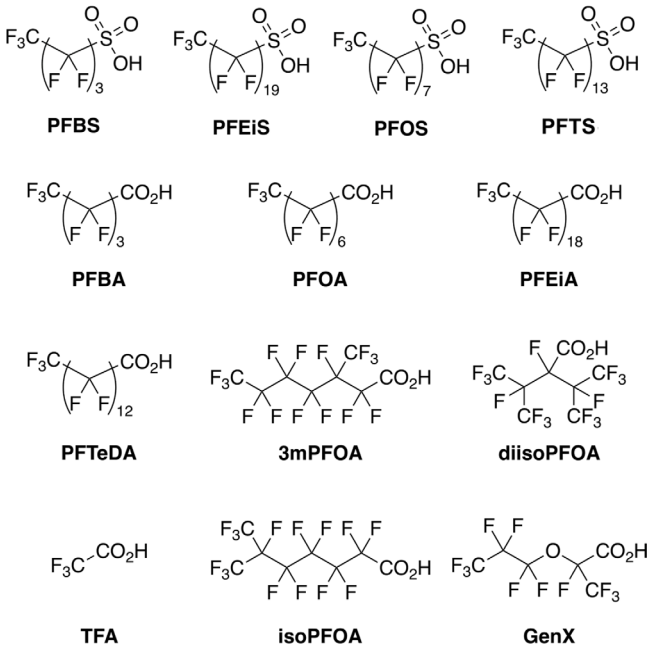

Fig. 2. Structural formulas of the PFAS investigated in this work.

Table 1
PFAS compounds and their acronyms.

Acronym	PFAS
PFBS	Perfluorobutanesulfonic acid
PFOS	Perfluoroottansulfonic acid
PFTS	Perfluorotetradecanesulfonic acid
PFEiS	Perfluoroeicosanesulfonic acid
PFBA	Perfluorobutanoic acid
PFOA	Perfluoroottanoic acid
PFTeDA	Perfluorotetradecanoic acid
PFEiA	Perfluoroeicosanoic acid
3mPFOA	3-methyl-perfluoroottanoic acid
isoPFOA	Isomethyl-perfluoroottanoic acid
diisoPFOA	Diisomethyl-perfluoroottanoic acid
TFA	Trifluoroacetic acid
GenX	Hexafluoropropylene oxide dimer acid

and Farré, 2021; Hildebrandt and Thünemann, 2023). Beyond their own effects, NP large surface area increases the likelihood of environmental contaminants, such as persistent organic pollutants, adsorbing onto their surfaces (Rai et al., 2022; Agboola and Benson, 2021; Qi and Qin, 2024; Sun et al., 2023; Tseng et al., 2022; Liu et al., 2019; Salawu et al., 2024; Cheng et al., 2021; Navarathna et al., 2023; Chen et al., 2023). This gives rise to co-transport phenomena that are particularly concerning, as they increase both the exposure of organisms to these contaminants and the probability that such pollutants reach drinking water sources (Cara et al., 2022; Cortés-Arriagada et al., 2023; Liu et al., 2023a). Pollutants adsorbed onto NPs can indeed be released into remote environments through the degradation of the polymer matrix (Jeong et al., 2018; Wang et al., 2019). This process contributes to the bioaccumulation of contaminants in aquatic organisms and leads to significant NP enrichment throughout the food chain, as described by Fig. 1 (Brandts et al., 2018; Koelmans et al., 2019; Chen et al., 2017a,b).

Due to their simultaneous presence in the aquatic ecosystems, it is crucial to understand how NPs and PFAS interact with each other, especially how they can give rise to co-transport phenomena that may significantly enhance their environmental impact. Despite its importance, the adsorption mechanism of PFAS onto nano and microplastics has been investigated in only few studies (Christian et al., 2022; Minervino and Belfield, 2024; Townsend, 2024; Liu et al., 2023b; Cortés-Arriagada, 2021; Enyoh et al., 2022), and, consequently, a detailed molecular-level understanding of this process is still lacking. The aim of this paper is to shed light, at an atomistic level, on the co-transport of PFAS and nanoparticles. To this end, we have carried out an extensive systematic computational study of the adsorption mechanism of a wide range of PFAS onto NPs made of polypropylene (PP), which is the second most widely used plastic in the world, along with PET (Koelmans et al., 2019). The structural formulas of the PFAS investigated in this work are shown in Fig. 2, while for the abbreviations of PFAS names refer to Table 1. We have recently demonstrated that PFOS rapidly adsorbs onto both the outer and inner surface of PPNPs, with the driving force of the adsorption process being the establishment of dispersion interactions between the adsorbent and the adsorbate (Simonetti et al., 2025). Here, our aim is to evaluate the influence of several factors on the adsorption mechanism: (i) the effect of the polar head group of PFAS, by conducting a comparative study of perfluorocarboxylic and perfluorosulfonic compounds; (ii) the effect of the perfluoroalkyl chain length, by varying the number of the chain carbon atoms; and (iii) the effect of branching, by analyzing three branched isomers of PFOA. Moreover, we have investigated the adsorption behavior of TFA and GenX, two PFAS of particular relevance: the former due to its extremely short perfluoroalkyl chain, and the latter because of its ether-bridge-containing dimeric structure, which is representative of next-generation replacement PFAS. To this end we have developed an *ad hoc* computational procedure, which consist of a combined approach that includes molecular mechanics computations based on classical force fields, semiempirical and electronic structure calculations based on DFT. By using such integrated approach we were able to describe quantitatively the adsorption mechanism of PFAS onto PPNPs, establishing trends in the adsorption behavior across a wide range of PFAS structural motifs.

2. Methods

2.1. Extended tight binding calculations

A model of PPNPs containing 422 atoms was constructed starting from a PP polymer chain consisting of 46 units (C_3H_6). The PPNP initial geometry was optimized by means of the GFN2-xTB method (Bannwarth et al., 2019). A conformational search was then performed using the CREST code (Pracht et al., 2020), in combination with the GFN-FF polarizable force field (Spicher and Grimme, 2020). The same procedure was repeated for the many PFAS-NP complexes. The most stable

structures obtained from the conformational sampling were optimized using the GFN2-xTB method in vacuum and in water by means of the Analytical Linearized Poisson Boltzmann (ALPB) approach (Ehlert et al., 2021). All the details of the computational procedure used in this work can be found in Section 3.1.

2.2. Quantum mechanical calculation details

The energies of the PFAS-PPNP complexes have been calculated using DFT by means of the Orca6 package (Neese, 2018). In particular both the energies and all of the other properties were computed adopting the all-electron def2-SVP basis set (Weigend and Ahlrichs, 2005) and the hybrid B3LYP functional (Becke, 1993). The energies have been calculated both in vacuum and in water simulating solvent effects by means of the CPCM formalism (Barone and Cossi, 1998). Dispersion force corrections were also included with the DFT-D3 method, together with the Becke–Johnson damping function (Grimme et al., 2011). The QM step of our multiscale protocol, performed at the B3LYP-D3/Def2-SVP level, is expected to have a typical accuracy of 1 kcal/mol for the adsorption energies, that is consistent with the well-established performance of this method for noncovalent interactions (Fishman et al., 2025).

The adsorption energies ΔE_{ads} have been calculated as:

$$\Delta E_{ads} = E_{PFAS\text{-}PPNP} - E_{PFAS} - E_{PPNP} \quad (1)$$

where $E_{PFAS\text{-}PPNP}$, E_{PFAS} and E_{PPNP} are the relaxed energies of the adsorption complex and of the isolated PFAS and PPNP, respectively.

Van der Waals potential (V_{vdW}) analysis was carried out to identify regions where dispersion interactions favor the stabilization of the adsorbate. In particular, VvdW is calculated as:

$$V_{vdW} = V_{repul} + V_{disp} \quad (2)$$

where V_{repul} and V_{disp} are the repulsion and dispersion potentials, respectively.

The nature of the interaction between the adsorbate and the NP has been evaluated by means of energy decomposition analysis based on absolutely localized molecular orbitals with implicit solvent (water) model, ALMO-EDA(solv) (Khaliullin et al., 2007, 2008). The ALMO-EDA analysis provides the interaction energy evaluated at the frozen complex geometry, denoted as:

$$\Delta E_{int} = \Delta E_{FRZ} + \Delta E_{POL} + \Delta E_{CT} \quad (3)$$

where ΔE_{POL} and ΔE_{CT} are the stabilizing energies due to polarization and charge transfer effects, respectively. ΔE_{FRZ} represents the interaction energy between the fragments when their electron densities are kept frozen as in the isolated monomers and it is given by:

$$\Delta E_{FRZ} = E_{ELEC} + E_{PAULI} + E_{DISP} \quad (4)$$

where E_{ELEC}, E_{PAULI} and E_{DISP} are the stabilizing energies due to intermolecular electrostatic interactions, Pauli repulsion and dispersion forces, respectively. To obtain the total adsorption energy, the fragment preparation energy (E_{prep}) must be included. Accordingly, the adsorption energy is now related to the interaction energy stemming from ALMO-EDA as:

$$\Delta E_{ads} = \Delta E_{int} + E_{prep} \quad (5)$$

where E_{prep} accounts for the deformation of the isolated fragments from their equilibrium geometries to those they adopt in the complex. The ALMO-EDA(solv) calculations were performed with the Q-Chem code (Shao et al., 2015).

Van der Waals potential (V_{vdW}) analysis was carried out to identify regions where dispersion interactions favor the stabilization of the adsorbate (Lu and Chen, 2020). In particular, V_{vdW} is calculated as:

$$V_{vdW} = V_{repul} + V_{disp} \quad (6)$$

where V_{repul} and V_{disp} are the repulsion and dispersion potentials, respectively. The nature of intermolecular interactions was also visualized using the Independent Gradient Model based on Hirshfeld partitioning (IGMH) (Lu and Chen, 2022), by means of Multiwfn 3.8 (Lu and Chen, 2012). The IGMH analyzes the electron density by partitioning its gradient into two terms (Rayene et al., 2022):

$$\delta g = \delta g_{intra} + \delta g_{inter} \quad (7)$$

where δg_{intra} and δg_{inter} are the intramolecular and intermolecular contributions, respectively. This method was employed to calculate the three-dimensional real space function δg_{inter}, whose color-filled maps allows one to highlight the different kind of interactions that are formed among the fragments.

3. Results and discussion

3.1. Development of the computational procedure

In order to describe the adsorption mechanism of PFAS compounds on PPNPs, we have carried out a comprehensive systematic study on a wide range of perfluoroalkyl sulfonic acids (PFSA) and perfluoroalkyl carboxylic acids (PFCA). It should be noted that the sulfonic and carboxylic head groups are predominantly dissociated under most environmental conditions. Accordingly, all calculations were performed using the deprotonated PFAS form. Simulating a large nanoparticle, large enough to form stable complexes also with long-chain PFAS, is essential for a study of this type but, in this way, the systems under investigation consist of nearly 500 atoms, making them prohibitively large for a full treatment using DFT methods. For this reason we have developed an *ad hoc* efficient, but accurate computational procedure especially suited for the systems under investigation. Our computational protocol integrates multiple levels of theory, combining classical force fields, semiempirical (SE) methods, and DFT calculations, each applied selectively at different stages of the procedure to balance accuracy and computational cost. In DFT energy calculations, one of the most computationally demanding steps is the iterative solution of the algebraic Kohn–Sham SCF problem, particularly for large systems. This computational cost can be significantly reduced by introducing semiempirical parameterizations into the matrix elements, thereby simplifying the underlying quantum mechanical problem. The resulting SE approaches retain a quantum mechanical framework, while simultaneously offering a notable computational advantage, delivering speed-ups of approximately two orders of magnitude compared to standard first-principles DFT methods (Christensen et al., 2016). Among semiempirical methods, tight-binding-based techniques, such as the GFNn-xTB family of universal parameterizations developed by Grimme have gained widespread adoption (Grimme et al., 2017; Bannwarth et al., 2019), particularly in high-throughput computational workflows. Despite their improved efficiency, SE methods still exhibit scaling limitations with respect to system size, which can restrict the scope of simulations to scales not vastly exceeding those accessible by full ab initio calculations (Bannwarth et al., 2021). As a result, performing extensive conformational searches on large systems may become computationally prohibitive even with SE methods. In such cases, it becomes necessary to resort to classical force field-based approaches, which allow for efficient exploration of conformational space at significantly lower computational cost.

Therefore, the computational procedure we have developed consists of the following steps:

- An initial reasonable geometry for the bare PPNP and all the PFAS-NP complexes have been initially optimized by means of the GFN2-xTB method.

- A conformational search of the bare PPNP and of the PFAS-NP systems has been performed through the use of CREST coupled with GFN-FF. This choice is motivated by the large size of the systems (~500 atoms), which would make the search process excessively time-consuming, even with a semiempirical method. In this case the non-covalent mode of the CREST method was employed, which enables the treatment of interactions between non-covalently bound fragments and allows one fragment to move relative to the other.
- All structures belonging to the conformational ensemble, within 6 kcal/mol above the lowest one, have been then screened and optimized in vacuum by using the semiempirical GFN2-xTB method, to overcome any limitation of the GFN-FF approach.
- The geometry in vacuum has been re-optimized including the presence of water as solvent.
- Finally, a single point energy calculation was performed on the lowest-lying PFAS-PPNP structure obtained in the preceding steps at a full DFT level and the interactions involved in the adsorption process have been thoroughly characterized.

To assess the reliability of our multiscale protocol, we further tested the computational workflow for two specific systems (PFOA and PFTS) by evaluating the DFT energy (B3LYP-D3/Def2-SVP) on ten optimized candidate structures from the GFN2 ensemble; the resulting energies at the DFT level showed a standard deviation of only 1.2 kcal mol^{-1}, indicating that the specific final structural choice has a limited impact on the reported results and that the protocol is solid and efficient in identifying (at least) one of the lowest lying conformers of the non-covalent complex. The raw data of the two tests are reported in Table S1 of the Supplementary Material.

With the exception of the conformational search of the bare PPNP, the computational procedure have been carried out three times starting from three different PFAS-PPNP initial structures, so that at the end, among all of the simulated configurations, for each investigated PFAS three PFAS-PPNP lowest-energy structures have been obtained.

3.2. The adsorption mechanism

Before studying the adsorption mechanism in detail, it is interesting to examine the surface characteristics of PPNPs. Fig. S1 of the Supplementary Material shows the electrostatic potential (ESP) map of the PPNP. In these map, red areas correspond to electron-rich regions with negative potential, whereas blue areas denote electron-deficient, positively charged zones. Since PP is a nonpolar material made up only of carbon and hydrogen, its charge distribution shows only limited polarity. The relatively low ESP range (−3.7 to 13.4 kcal/mol) reflects a weak surface charge overall. Conversely, in general PFAS are characterized by a hydrophobic perfluorinated tail and a hydrophilic head group, enabling them to function effectively as surfactants. The highly fluorinated alkyl chain promotes hydrophobic interactions and resists mixing with water, thus favoring adsorption onto nonpolar materials. Moreover, the anionic head group can form electrostatic interactions with oppositely charged particles. Fig. S2 of the Supplementary Material shows the electrostatic potential (ESP) map of PFOA and PFOS, as an example. The maps obtained for the two compounds are very similar to each other: the negatively charged domains shown in peach highlights their propensity for electrostatic interactions with the slightly positively charged regions of the PP nanoparticles. However, since the nanoplastic carries only a very weak positive charge, the electrostatic contribution to the interactions between the adsorbate and the adsorbent plays a minor role, while dispersive forces represent the dominant interactions (*vide infra*).

PFOS is an eight-carbon molecule characterized by an oleophobic perfluorinated tail and a hydrophilic head group, enabling it to function effectively as a surfactant. Its sulfonic acid moiety remains largely dissociated under most environmental and biological conditions (pKa < 1). The highly fluorinated alkyl chain promotes hydrophobic interactions and resists mixing with water, thus favoring adsorption onto nonpolar materials (Rayne and Forest, 2009; Pontius, 2019; He et al. 2024). Moreover, the anionic head group can form electrostatic associations with oppositely charged particles. The electrostatic potential (ESP) maps of PFOS highlights these negatively charged domains in red, revealing its propensity for non-covalent interactions with positively charged regions on PP nanoparticles.

Moreover, we calculated the solvent accessible surface area (SASA) of the nanoparticle using VMD, obtaining a value of 1817 $Å^2$. This parameter represents the total surface area accessible to solvent molecules and provides an estimate of the available surface that can interact with the adsorbates. In order to identify the regions of the nanoparticle prone to contaminant physisorption, it is useful to analyze the V_{vdW}, which is shown in Fig. S3 of the Supplementary Material. V_{vdW} negative zones are colored orange, showing the regions around the PPNP where attractive dispersion forces will surpass exchange repulsion effects. Therefore, in such regions adsorbate molecules can be adsorbed via dispersion forces.

The three PFAS-PPNP structures (labeled as C1, C2 and C3), corresponding to the three lowest-energy configurations, are reported in Fig. 3 for the PFAS listed in Fig. 2. To better visualize the interactions formed between the two fragments in the complex, the nanoparticle has been represented by using the VMD QuickSurf algorithm. The geometry of the optimized structures in water were very similar to those in vacuum. We have therefore decided to show only the final structures obtained from the in water calculations. A detailed comparison of the adsorption energies obtained in vacuum and in water is provided in the Supplementary Material. An important finding which emerges from visual inspection of the obtained structures is that the geometry of the NP varies depending on the positioning and binding orientation of the PFAS molecule. The PPNP shows indeed a very large flexibility that allows it to change in shape and to adapt in such a way to accommodate the adsorbate molecule. It rearranges itself in a different way in each configuration in order to maximize the specific interactions with the PFAS molecule. The ability of the PPNP to be so adaptable to the local environment, in this case the specific adsorbate, allows it to form interactions with the entire PFAS molecule even when it possesses a very long perfluorinated chain. A striking example of this behavior is given by the PFEiA compound, that is able to fully extend itself on the nanoparticle surface.

The entire set of adsorption energies for all of the optimized structures in water are listed in Table S2 of the Supplementary Material and they are shown in Fig. 4. The negative adsorption energy values obtained for all the PFAS compounds indicate the formation of stable complexes. They are comparable with the energies previously found for other adsorbents on polymer micro- and nanoparticles (Cortés-Arriagada, 2021; Cortés-Arriagada et al., 2023; Enyoh et al., 2022). Our computational results are in good qualitative agreement with the experimental observations reported by Ateia et al. (2020). Both the observations reported in that study and the present computational evidence clearly indicate that PFSAs exhibit a stronger affinity for polymeric surfaces than their PFCA counterparts of comparable chain length. This trend can be attributed to the combination of larger dispersion contribution to the binding energies (closely related to a higher hydrophobicity in the experiments) and to the stronger electrostatic forces arising from the sulfonate group, as shown by EDA. Also, we can observe that the adsorption strength systematically increases with the length of the perfluoroalkyl chain, in line with the experimental observations that long-chain PFAS display greater sorption capacities than short-chain analogues. Again, it is evident how the increase of dispersion interactions between the fluorocarbon chain and the polymer matrix acts as the main drive of hydrophobicity. Our results point to the plasticity of the polymer substrate surface and to dispersion interactions as the main stabilizing contributions, with secondary but non-negligible electrostatic effects that are particularly pronounced for

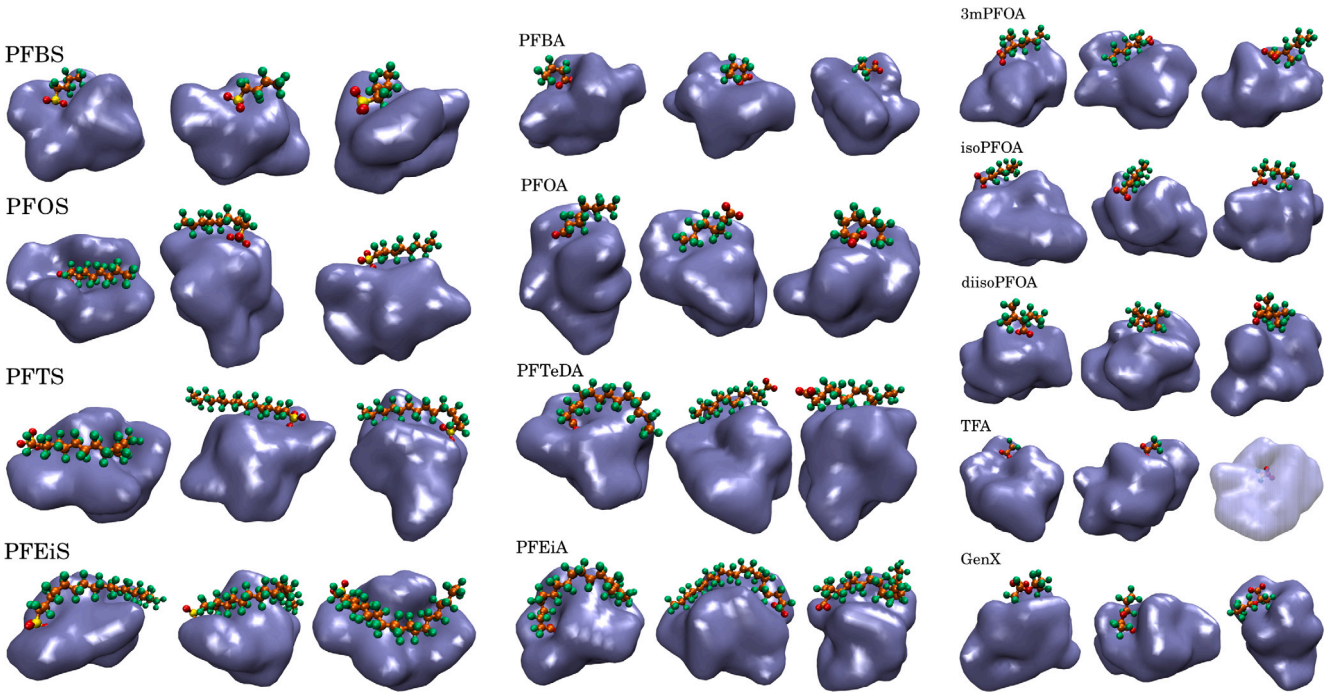

Fig. 3. Molecular structures of the PFAS-PPNPs complexes C1 (left panels), C2 (middle panels) and C3 (right panels) obtained from the geometry optimization procedure for all of the PFAS compound investigated in this work.

sulfonates. This agrees with the experimental interpretation of Ateia et al. who ascribed the enhanced sorption of real microplastics to, among other, surface roughness, and local charges, all of which can be rationalized in molecular terms as a combination of steric, dispersion and auxiliary electrostatic interactions (Ateia et al., 2020). There is another additional point of contact between our model and the observations that is worth underlining: our calculations show a significantly lower adsorption energy for highly branched, long-chain sulfonates such as PFEiS, while Ateia et al. also noted that sorption trends are not strictly linear with chain length (Ateia et al., 2020). This overall consistency between theory and experiment strengthens the reliability of our description of the mechanistic understanding of PFAS adsorption on polymeric substrates.

First of all, it is useful to compare the behavior of the adsorption energies computed for the same PFAS adsorbate. There is a certain variability of the energies associated to the three structures C1, C2 and C3. In particular, the largest differences are found for long-chain PFAS, showing also the largest energy values, such as PFTS and PFEiA whose difference between C1 and C3 adsorption energies are 18.3 and 22.7 kcal/mol, respectively. However, in some cases very similar interaction energies are obtained for the different structures, even if from a structural point of view the corresponding configurations are very different from each other, as it can be observed, as an example, for configurations C1 and C2 of PFBS or PFBA, and configurations C2 and C3 of PFTeDA.

Several studies suggest that the co-transport of contaminants can occur on both the outer and inner surfaces of polymeric nanoparticles (Cortés-Arriagada, 2021). Moreover, it has been observed experimentally that small PFAS molecules can partially diffuse into the material's pores (Salawu et al., 2024). It is therefore interesting, for each adsorbed PFAS, to determine if there is a preference for either inner or outer adsorption on PPNPs. It is important to stress that here the definition of inner and outer adsorption is not a strict definition, since it descends from a visual inspection of the obtained structures. As a general trend, all of the investigated compounds exhibits both inner (or partially inner) and outer adsorption on PPNP. The only exception to this behavior is represented by TFA, which is adsorbed only on the inner surface of the PPNP, and in one of the three configurations (C3) it is even incorporated into the nanoparticle. In this respect, TFA thus shows a very different behavior as compared to the other PFAS systems, as a consequence of its very little molecular volume. In most cases, the most stable configuration C1 corresponds to an inner adsorption. On the other hand, PFTS, PFOA, 3mPFOA, diisoPFOA and GenX prefer to adsorb on the outer surface of the PPNP nanoparticle. It is not simple to bring to light a general behavior for the different PFAS to form either an inner or outer adsorption complex. As an example, taking into account the same chain composed of eight carbon atoms, PFOS and PFOA prefer to be adsorbed on the inner and outer surface of the nanoparticle, respectively.

It is interesting to compare the lowest energy values, corresponding to the most representative configuration of each PFAS systems (C1), obtained for the two classes of PFAS compounds investigated in this work, namely PFSA and PFCA, as a function of the PFAS perfluorinated chain length (see Fig. 5). As a general trend, for a given number of carbon atoms of the perfluorinated chain, PFSA always show larger adsorption energies ad compared to the corresponding PFCA. This behavior is in line with the results of Zenobio et al. that found stronger adsorption of PFAS sulfonates than analogous carboxylates to PP containers (Zenobio et al., 2022). Such a peculiar behavior has been ascribed by the authors to their greater hydrophobicity (Zenobio et al., 2022). By looking at the trend obtained for PFCA, we can see that the adsorption energies increase as the PFAS perfluorinated chain length increases. This increase can be explained by the increase of the number of possible interactions among the PFAS and the PPNP interactions sites. We have indeed shown that the PPNP is able to adapt and rearrange itself to maximize the interactions with the adsorbate. As a consequence, we can expect that the more the possible interaction sites, the more the adsorption energy. This result is in line with the fact that the driving force of the adsorption process is the formation of dispersion forces between the PFAS perfluorinated chain and the NP alkyl chain (*vide infra*). The PFSA adsorption energies show the same regular trend observed for PFCA as a function of the number of perfluorinated chain carbon atoms up to a

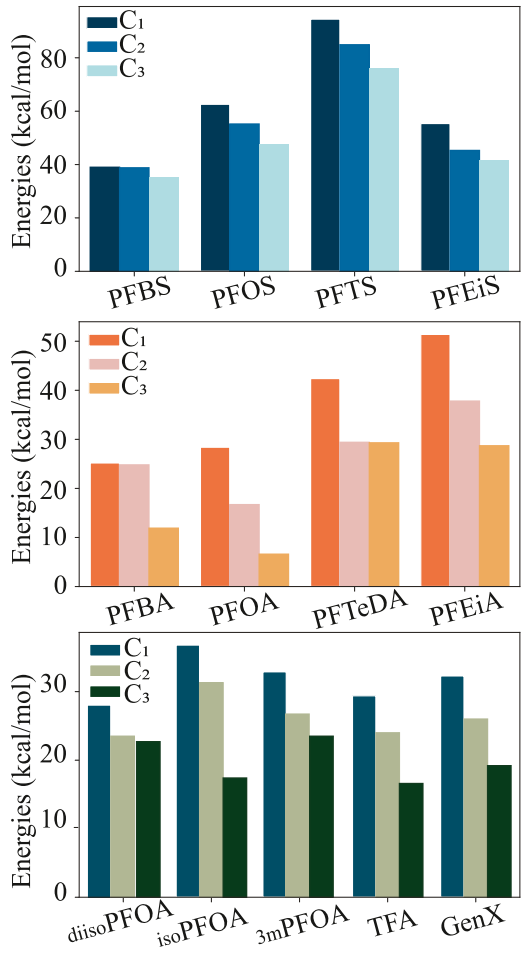

Fig. 4. Absolute value of the adsorption energies, shown as bar plots, calculated in water for all the investigated PFAS-PPNP complexes.

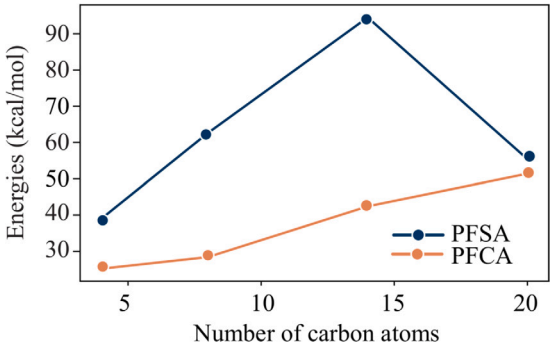

Fig. 5. Absolute value of the adsorption energies corresponding to the C1 configuration of each PFAS-PPNP complex, obtained for the two classes of PFAS compounds investigated in this work, namely PFSA and PFCA, as a function of the number of carbon atoms of the PFAS perfluorinated chain.

number of carbon atoms of 14, corresponding to the PFTS system, while decreasing for the last member of the series (PFEiS). Therefore, even if the PPNP adjusts itself to maximize the interactions with the PFAS molecule, such interactions in PFEiS are not as strong as those formed by the shorter chain counterparts. Note that among PFSA containing systems, PFTS has the largest adsorption energies of all the compounds investigated in this work (94.5 kcal/mol).

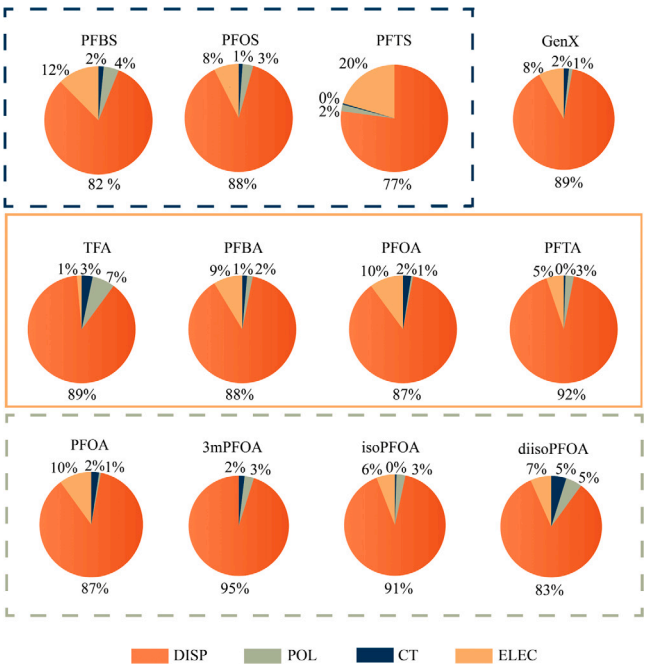

Fig. 6. Percentage contributions of ALMO-EDA terms in the C1 configuration of selected PFAS-PPNP complexes. ELEC, DISP, POL and CT refer to the stabilizing energies due to intermolecular electrostatic, dispersion forces, polarization and charge transfer effects, respectively.

Finally, if we look at the adsorption energies of the C1 configuration of the three isomers of PFAS obtained by varying the branching of the perfluorinated chain (3mPFOA, isoPFOA and diisoPFOA), we can see that in all cases they are larger than to the linear isomer. This is a very peculiar result which is in contrast with the findings reported by Kleiner et al. for PFAS adsorbed on high-density polyethylene (HDPE) surfaces (Kleiner et al., 2021). However, this is not surprising since in the study the adsorption occurs on a surface which, although potentially porous, remains static and lacks the flexibility and adaptability exhibited by the NPs investigated in the present work. Owing to their properties, NPs are indeed capable of forming strong interactions even in presence of a large steric hindrance caused by the branching of the polymer chain.

3.3. The nature of the interactions

At this point it is interesting to shed light on the driving forces governing the adsorption process. To this end, it is useful to investigate the specific contribution of the stabilizing interactions involved in the binding between PFAS and PPNP, by decomposing the interaction energy of the configuration C1 of selected PFAS using the ALMO-EDA(solv) method. The results are shown in Fig. 6. The main destabilizing contribution within the complexes arises from Pauli repulsion. These destabilizing effects are more than offset by stabilizing interactions, with dispersion forces playing the dominant role, leading to an overall favorable adsorption process and positive net adsorption energies for all complexes. The driving force of the adsorption process is thus in all cases the formation of dispersion interactions between the adsorbent and the adsorbate. In addition to dispersion interactions (DISP in Fig. 6), PFAS and NPs also interact through electrostatic forces (ELEC in Fig. 6), even if to a much lesser extent. The electrostatic contribution is generally more pronounced in PFSA as compared to PFCA. Of particular interest is the remarkably high electrostatic contribution (20%) observed in the PFTS complex, which also exhibits the highest adsorption energy value among all of the studied systems. Interestingly,

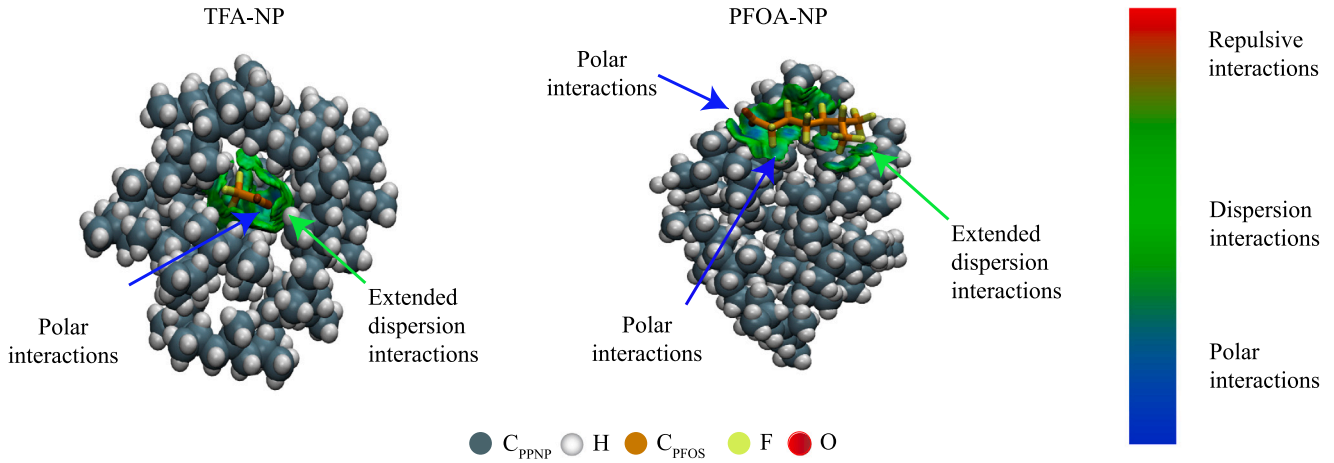

Fig. 7. Independent gradient model based on Hirshfeld partitioning (IGMH) analysis of non-covalent intermolecular interactions taking place in the TFA- and PFOA-PPNP complexes. (For interpretation of the references to color in this figure legend, the reader is referred to the web version of this article.)

TFA exhibits a higher polarization contribution as compared to the other compounds, which can be attributed to its higher charge density. This is likely due to its low molecular weight, which results in a more localized charge density, and therefore a higher polarizing power relative to the other members of the carboxylate series.

Finally, intermolecular interactions were analyzed using the IGMH approach (Lu and Chen, 2022). Fig. S5, S6 and S7 of the Supplementary Material displays the δg_{inter} isosurfaces calculated for the three configurations of all the PFAS-PPNP complexes investigated in this work, namely PFSA, PFCA and the branched isomers of PFOA (together with GenX and TFA), respectively. Fig. 7 shows selected configurations of the TFA and PFOA compounds. Blue and green regions highlight regions where polar interactions and dispersion forces occur, respectively. Dispersion interactions are confirmed to be the predominant stabilizing forces across all complexes, in agreement with the ALMO-EDA(solv) analysis. Such dispersion interactions are formed at the interface between the NP and the contaminant, all along the perfluorinated chain of the PFAS compound.

An interesting point to note is that, although short-chain PFAS exhibit higher polarity compared to long-chain PFAS, physical inner adsorption can still occur (Liu et al., 2018). As shown in Fig. 7, in the specific case of TFA, the shortest-chain PFAS, the compound in the C3 configuration is completely adsorbed within the NP, in contrast to longer-chain PFAS such as PFOA, also depicted in the same figure. As previously observed by Cortés-Arriagada for BPA adsorption on nanoPET (Cortés-Arriagada, 2021), this result demonstrates that physical entrapment of TFA molecules is possible within the inner surface of PPNPs. This behavior is primarily attributed to dispersion forces, which stabilize the complex and dominate the inner adsorption process. Our results suggest that the preferential adsorption of TFA onto the inner surfaces of microplastics may significantly influence its toxicokinetic behavior, potentially increasing its bioavailability and altering its overall toxicological profile.

4. Conclusions

In this paper a thorough systematic investigation of the adsorption mechanism of a variety of PFAS onto PPNPs has been carried out. To this end, we developed a computational procedure that integrates molecular mechanics using classical force fields, SE methods, and electronic structure calculations based on DFT. This comprehensive approach enabled us to shed light on the driving force governing the adsorption process, revealing for the first time similarities and differences in the adsorption behavior as a function of the PFAS structural features, in particular the length and branching of the perfluoroalkyl chain, as well as the variation of the head group from carboxylate to sulfonate. All of the investigated PFAS are able to adsorb onto the PPNP, as evidenced by their positive adsorption energies. This ability to adsorb onto PPNP has serious environmental implications, as it facilitates transport phenomena that can enhance PFAS exposure and promote their dispersion over long distances. Such processes are particularly concerning due to the potential for biomagnification through the food chain, posing risks to ecosystems and human health. Our findings suggest that the local flexibility of the NP is the key factor enabling an effective adsorption of all the investigated PFAS compounds. Indeed, the PPNP structure undergoes different rearrangements in each PFAS complex to maximize the intermolecular interactions. The adsorption mechanism is mainly driven by the establishment of dispersion forces between the PFAS perfluorinated chain and the NP alkyl chain, with electrostatic interactions giving a minor contribution to the complex stabilization. Almost all of the studied compounds exhibit both internal and external adsorption, with internal adsorption generally being the more favorable one. As a general trend, perfluorosulfonic acids exhibit larger adsorption energies as compared to their carboxylic acids counterpart, and the PFAS-PPNP interaction becomes stronger with increasing the length of the perfluoroalkyl chain, as more and more dispersion forces can be established between the two fragments. Increasing the branching of the PFAS chain leads to higher adsorption energies. This peculiar behavior can be attributed to the remarkable adaptability of the NP, which allows it to interact effectively with the PFAS molecule even in the presence of increased steric hindrance caused by chain branching. This work constitutes a first step toward a comprehensive understanding of the complex mechanisms taking place in real aquatic environments. The theoretical calculations reported herein were performed on an ideal model system consisting exclusively of water continuum model and the adsorption complex with a single PFAS. Future investigations should aim to address multi-molecule adsorption using larger-scale simulations. In this way, it will be possible to better describe the real environmental conditions of aqueous basins and thus capture more effectively the inherent complexity and variability of the real systems.

These findings can be of great help in the rationalization of PFAS adsorption behavior, which represents a crucial step toward addressing this major environmental and public health emergency. A molecular-level understanding of the co-transport of PFAS and NPs not only helps clarifying their environmental fate and transport but it also provides valuable insights for the development of effective strategies for PFAS removal from contaminated water sources.

CRediT authorship contribution statement

Valentina Migliorati: Writing – review & editing, Writing – original draft, Visualization, Supervision, Software, Methodology, Data curation, Conceptualization. **Federica Simonetti:** Visualization, Methodology, Investigation, Data curation, Conceptualization. **Luca Bertagnin:** Methodology, Investigation, Data curation. **Enrico Bodo:** Writing – review & editing, Writing – original draft, Visualization, Supervision, Software, Methodology, Data curation, Conceptualization.

Declaration of competing interest

The authors declare that they have no known competing financial interests or personal relationships that could have appeared to influence the work reported in this paper.

Acknowledgments

We acknowledge the CINECA award under the ISCRA initiative, for the availability of high-performance computing resources and support. In particular, the support by the CINECA supercomputing centers has been obtained through the grant IscrC_ODISSEY (n. HP10CZCTEF). Moreover, the work was supported from the University of Rome "La Sapienza", Italy (Progetto ateneo Grant. RG123188B163C1B6).

Appendix A. Supplementary data

Section "Comparison of the adsorption energies obtained in vacuum and in water". Table S1-S2 and Figures S1-S7.

Supplementary material related to this article can be found online at https://doi.org/10.1016/j.envpol.2025.127434.

Data availability

Data will be made available on request.

References

Agboola, O., Benson, N., 2021. Physisorption and chemisorption mechanisms influencing micro (nano) plastics-organic chemical contaminants interactions: A review. Front. Env. Sci 9, 678574.

Ateia, M., Zheng, T., Calace, S., Tharayil, N., Pilla, S., Karanfil, T., 2020. Sorption behavior of real microplastics (mps): Insights for organic micropollutants adsorption on a large set of well-characterized mps. Sci. Total. Env. 720, 137634.

Bannwarth, C., Caldeweyher, E., Ehlert, S., Hansen, A., Pracht, P., Seibert, J., Spicher, S., Grimme, S., 2021. Extended tight-binding quantum chemistry methods. Wiley Interdiscip. Rev. Comput. Mol. Sci. 11, e1493.

Bannwarth, C., Ehlert, S., Grimme, S., 2019. Gfn2-xtb2014an accurate and broadly parametrized self-consistent tight-binding quantum chemical method with multipole electrostatics and density-dependent dispersion contributions. J. Chem. Theory Comput. 15, 1652–1671.

Barone, V., Cossi, M., 1998. Quantum calculation of molecular energies and energy gradients in solution by a conductor solvent model. J. Phys. Chem. A 102, 1995–2001.

Becke, A.D., 1993. A new mixing of hartree–fock and local density-functional theories. J. Chem. Phys. 98, 1372–1377.

Bergmann, M., Collard, F., Fabres, J., Gabrielsen, G.W., Provencher, J.F., Rochman, C.M., Sebille, E.van., Tekman, M.B., 2022. Plastic pollution in the arctic. Nat. Rev. Earth. Env. 3, 323–337.

Brandts, I., Teles, M., Goncalves, A., Barreto, A., Franco-Martinez, L., Tvarijonaviciute, A., Martins, M., Soares, A., Tort, L., Oliveira, M., 2018. Effects of nanoplastics on mytilus galloprovincialis after individual and combined exposure with carbamazepine. Sci. Total. Env. 643, 775–784.

Cara, B., Lies, T., Thimo, G., Robin, L., Lieven, B., 2022. Bioaccumulation and trophic transfer of perfluorinated alkyl substances (pfas) in marine biota from the belgian north sea: Distribution and human health risk implications. Environ. Pollut. 311, 119907.

Chen, Q., Gundlach, M., Yang, S., Jiang, J., Velki, M., Yin, D., Hollert, H., 2017a. Quantitative investigation of the mechanisms of microplastics and nanoplastics toward zebrafish larvae locomotor activity. Sci. Total. Env. 584- 585, 1022–1031.

Chen, X., Qadeer, A., Liu, M., Deng, L., Zhou, P., Mwizerwa, I.T., Liu, S., Ajmal, Z., Xingru, Z., Jiang, X., 2023. Chapter 13 - bioaccumulation of emerging contaminants in aquatic biota: Pfas as a case study. In: Kumar, M., Mohapatra, S., Weber, K. (Eds.), Emerging Aquatic Contaminants. pp. 347–374.

Chen, Q., Yin, D., Jia, Y., Schiwy, S., Legradi, J., Yang, S., Hollert, H., 2017b. Enhanced uptake of bpa in the presence of nanoplastics can lead to neurotoxic effects in adult zebrafish. Sci. Total. Env. 609, 1312–1321.

Cheng, Y., Mai, L., Lu, X., Li, Z., Guo, Y., Chen, D., Wang, F., 2021. Occurrence and abundance of poly-and perfluoroalkyl substances (pfass) on microplastics (mps) in pearl river estuary (pre) region: Spatial and temporal variations. Environ. Pollut. 281, 117025.

Christensen, A.S., T., Kubaň159, Cui, Q., Elstner, M., 2016. Semiempirical quantum mechanical methods for noncovalent interactions for chemical and biochemical applications. Chem. Rev. 116, 5301–5337.

Christian, E.E., Qingyue, W., Weiqian, W., Tanzin, C., Mominul, H.R., Rezwanul, I., Guo, Y., Lin, Y., Kai, X., 2022. Sorption of per- and polyfluoroalkyl substances (pfas) using polyethylene (pe) microplastics as adsorbent: Grand canonical monte carlo and molecular dynamics (gcmc-md) studies. J. Env. Anal. Chem 1–17.

Cortés-Arriagada, D., 2021. Elucidating the co-transport of bisphenol a with polyethylene terephthalate (pet) nanoplastics: A theoretical study of the adsorption mechanism. Environ. Pollut. 270, 116192.

Cortés-Arriagada, D., Miranda-Rojas, M.B., Ortega, D.E., Alarcón-Palacio, V.B., 2023. The interaction mechanism of polystyrene microplastics with pharmaceuticals and personal care products. Sci. Total. Env. 861, 160632.

Cousins, I.T., Johansson, J.H., Salter, M.E., Sha, B., Scheringer, M., 2022. Outside the safe operating space of a new planetary boundary for per- and polyfluoroalkyl substances (pfas). Res. J. Env. Toxicol 56, 11172–11179.

Deep, S., Ahluwalia, J.C., 2001. Interaction of bovine serum albumin with anionic surfactants. Phys. Chem. Chem. Phys 3, 4583–4591.

Ehlert, S., Stahn, M., Spicher, S., Grimme, S., 2021. Robust and efficient implicit solvation model for fast semiempirical methods. J. Chem. Theory Comput. 17, 4250–4261.

Enfrin, M., Dumée, L.F., Lee, J., 2019. Nano/microplastics in water and wastewater treatment processes – origin. Impact Potential Solutions. Water Res 161, 621–638.

Enyoh, C.E., Wang, Q., Wang, W., Chowdhury, T., Rabin, M.H., Islam, R., Yue, G., Yichun, L., Xiao, K., 2022. Sorption of per-and polyfluoroalkyl substances (pfas) using polyethylene (pe) microplastics as adsorbent: Grand canonical monte carlo and molecular dynamics (gcmc-md) studies. J. Env. Anal. Chem 104, 1–17.

Fenton, S.E., Ducatman, A., Boobis, A., DeWitt, J.C., Lau, C., Ng, C., Smith, J.S., Roberts, S.M., 2021. Per-and polyfluoroalkyl substance toxicity and human health review: Current state of knowledge and strategies for informing future research. Environ. Toxicol. Chem. 40, 606–630.

Fishman, V., Lesiuk, M., Martin, J.M.L., Daniel Boese, A., 2025. Another angle on benchmarking noncovalent interactions. J. Chem. Theory Comput. 21, 2311–2324.

Gigault, J., ter Halle, A., Baudrimont, M., Pascal, P.Y., Gauffre, F., Phi, T.L., El Hadri, B., Reynaud, S., 2018. Current opinion: What is a nanoplastic? Environ. Pollut 235, 1030–1034.

Grimme, S., Bannwarth, C., Shushkov, P., 2017. A robust and accurate tight-binding quantum chemical method for structures, vibrational frequencies, and noncovalent interactions of large molecular systems parametrized for all spd-block elements (z = 1ž01386). J. Chem. Theory Comput. 13, 1989–2009.

Grimme, S., Ehrlich, S., Goerigk, L., 2011. Effect of the damping function in dispersion corrected density functional theory. J. Comput. Chem. 32, 1456–1465.

Hernando, M.D., Mezcua, M., A.F.A.D.B., 2006. Environmental risk assessment of pharmaceutical residues in wastewater effluents. Surf. Waters Sediments. Talanta 69, 334–342.

Hildebrandt, J., Thünemann, A.F., 2023. Aqueous dispersions of polypropylene: toward reference materials for characterizing nanoplastics. Macromol. Rapid Comm 44, 2200874.

Jeong, C.B., Kang, H.M., Lee, Y.H., Kim, M.S., Lee, J.S., Seo, J.S., Wang, M., Lee, J.S., 2018. Nanoplastic ingestion enhances toxicity of persistent organic pollutants (pops) in the monogonont rotifer brachionus koreanus via multixenobiotic resistance (mxr) disruption. Res. J. Env. Sci. Toxicol 52, 11411–11418.

Joo, S.H., Liang, Y., Kim, M., Byun, J., Choi, H., 2021. Microplastics with adsorbed contaminants: Mechanisms and treatment. Env. Chall 3, 100042.

Khaliullin, R.Z., Bell, A.T., Head-Gordon, M., 2008. Analysis of charge transfer effects in molecular complexes based on absolutely localized molecular orbitals. J. Phys. Chem. 128.

Khaliullin, R.Z., Cobar, E.A., Lochan, R.C., Bell, A.T., Head-Gordon, M., 2007. Unravelling the origin of intermolecular interactions using absolutely localized molecular orbitals. J. Phys. Chem. 111, 8753–8765.

Kleiner, E.J., Sanan, T., Smith, S.J., Pressman, J.G., Abulikemu, G., Crone, B.C., Wahman, D.G., 2021. Practical implications of perfluoroalkyl substances adsorption on bottle materials: Isotherms. AWWA Water Sci. 3, e1243.

Koelmans, A.A., Mohamed Nor, E., Kooi, M., Mintenig, S.M., De France, J., 2019. Microplastics in freshwaters and drinking water: Critical review and assessment of data quality. Water Res. 155, 410–422.

Kurwadkar, S., Dane, J., Kanel, S.R., Nadagouda, M.N., Cawdrey, R.W., Ambade, B., Struckhoff, G.C., Wilkin, R., 2022. Per-and polyfluoroalkyl substances in water and wastewater: A critical review of their global occurrence and distribution. Sci. Total. Env. 809, 151003.

Liu, J., Ma, Y., Zhu, D., Xia, T., Qi, Y., Yao, Y., Guo, X., Ji, R., Chen, W., 2018. Polystyrene nanoplastics-enhanced contaminant transport: role of irreversible adsorption in glassy polymeric domain. Environ. Sci. Technol. 52, 2677–2685.

Liu, W., Tang, H., Yang, B., Li, C., Chen, Y., Huang, T., 2023a. Molecular level insight into the different interaction intensity between microplastics and aromatic hydrocarbon in pure water and seawater. Sci. Total. Env. 862, 160786.

Liu, W., Tang, H., Yang, B., Li, C., Chen, Y., Huang, T., 2023b. Molecular level insight into the different interaction intensity between microplastics and aromatic hydrocarbon in pure water and seawater. Sci. Total. Env. 862, 160786.

Liu, G., Zhu, Z., Yang, Y., Sun, Y., Yu, F., Ma, J., 2019. Sorption behavior and mechanism of hydrophilic organic chemicals to virgin and aged microplastics in freshwater and seawater. Environ. Pollut. 246, 26–33.

Llorca, M., Farré, M., 2021. Current insights into potential effects of micro-nanoplastics on human health by in-vitro tests. Front. Toxicol 3, 752140.

Lu, T., Chen, F., 2012. Multiwfn: A multifunctional wavefunction analyzer. J. Comput. Chem. 33, 580–592.

Lu, T., Chen, Q., 2020. Van der waals potential: an important complement to molecular electrostatic potential in studying intermolecular interactions. J. Mol. Model. 26 (315).

Lu, T., Chen, Q., 2022. Independent gradient model based on hirshfeld partition: A new method for visual study of interactions in chemical systems. J. Comput. Chem. 43, 539–555.

Minervino, A., Belfield, K.D., 2024. Review of recent computational research on the adsorption of pfass with a variety of substrates. Int. J. Mol. Sci. 25 (3445).

Navarathna, C.M., Pray, H., Rodrigo, P.M., Arwenyo, B., McNeely, C., Reynolds, H., Hampton, N., Lape, K., Roman, K., Heath, M., et al., 2023. Microplastics and per- and polyfluoroalkyl substances (pfas) analysis in sea turtles and bottlenose dolphins along mississippi's coast. Analytica 4, 12–26.

Neese, F., 2018. Software update: the orca program system, version 4.0. WIREs Comput. Mol. Sci. 8, e1327.

Pelegrini, K., Pereira, T.C.B., Maraschin, T.G., Teodoro, L.D.S., Basso, N.R.D.S., De Galland, R.A., Bogo, M.R., 2023. Micro- and nanoplastic toxicity: A review on size, type, source, and test-organism implications. Sci. Total Environ. 878, 162954.

Peng, L., Fu, D., Qi, H., Lan, C.Q., Yu, H., Ge, C., 2020. Micro- and nano-plastics in marine environment: Source, distribution and threats — a review. Sci. Total Environ. 698, 134254.

Pizzini, S., Giubilato, E., Morabito, E., Barbaro, E., Bonetto, A., Calgaro, L., Feltracco, M., Semenzin, E., Vecchiato, M., Zangrando, R., Gambaro, A., Marcomini, A., 2024. Contaminants of emerging concern in water and sediment of the venice lagoon, italy. Environ. Res. 249, 118401.

Podder, A., Sadmani, A.A., Reinhart, D., Chang, N.B., Goel, R., 2021. Per and polyfluoroalkyl substances (pfas) as a contaminant of emerging concern in surface water: A transboundary review of their occurrences and toxicity effects. J. Hazard. Mater 419, 126361.

Pracht, P., Bohle, F., Grimme, S., 2020. Automated exploration of the low-energy chemical space with fast quantum chemical methods. Phys. Chem. Chem. Phys 22, 7169–7192.

Qi, L., Qin, W., 2024. Unveiling the fast adsorption and desorption of heavy metals on/off nanoplastics by real-time in-situ potentiometric sensing. Sci. Total. Env. 943, 173789.

Rai, P.K., Sonne, C., Brown, R.J., Younis, S.A., Kim, K.H., 2022. Adsorption of environmental contaminants on micro- and nano-scale plastic polymers and the influence of weathering processes on their adsorptive attributes. J. Hazard. Mater 427, 127903.

Rayene, K., Imane, D., Abdelaziz, B., Leila, N., Fatiha, M., Abdelkrim, G., Bouzid, G., Ismahan, L., Brahim, H., Rabah, O., 2022. Molecular modeling study of structures, hirschfield surface, nbo, aim, rdg, igm and 1hnmr of thymoquinone/hydroxypropyl-β-cyclodextrin inclusion complex from qm calculations. J. Mol. Struct. 1249, 131565.

Salawu, O.A., Olivares, C.I., Adeleye, A.S., 2024. Adsorption of pfas onto secondary microplastics: A mechanistic study. J. Hazard. Mater 470, 134185.

Sandoval, M.A., Calzadilla, W., Vidal, J., Brillas, E., Salazar-González, R., 2024. Contaminants of emerging concern: Occurrence, analytical techniques, and removal with electrochemical advanced oxidation processes with special emphasis in latin america. Environ. Pollut. 345, 123397.

Shao, Y., Gan, Z., Epifanovsky, E., Gilbert, A.T., Wormit, M., Kussmann, J., Lange, A.W., Behn, A., Deng, J., Feng, X., et al., 2015. Advances in molecular quantum chemistry contained in the q-chem 4 program package. Mol. Phys. 113, 184–215.

Simonetti, F., Mancini, M., Gioia, V., Zumpano, R., Mazzei, F., Frugis, A., Migliorati, V., 2025. Unveiling the adsorption mechanism of perfluorooctane sulfonate onto polypropylene nanoplastics: A combined theoretical and experimental investigation. Water Res. 278, 123324.

Spicher, S., Grimme, S., 2020. Robust atomistic modeling of materials, organometallic, and biochemical systems. Angew. Chem. Int. Ed. 59, 15665–15673.

Sun, N., Shi, H., Li, X., Gao, C., Liu, R., 2023. Combined toxicity of micro/nanoplastics loaded with environmental pollutants to organisms and cells: Role, effects, and mechanism. Environ. Int. 171, 107711.

Townsend, P.A., 2024. Adsorption in action: Molecular dynamics as a tool to study adsorption at the surface of fine plastic particles in aquatic environments. ACS Omega 9, 5142–5156.

Tseng, L.Y., You, C., Vu, C., Chistolini, M.K., Wang, C.Y., Mast, K., Luo, F., Asvapathanagul, P., Gedalanga, P.B., Eusebi, A.L., Gorbi, S., Pittura, L., Fatone, F., 2022. Adsorption of contaminants of emerging concern (cecs) with varying hydrophobicity on macro- and microplastic polyvinyl chloride, polyethylene, and polystyrene: Kinetics and potential mechanisms. Water 14.

Wang, Q., Tsui, M.M., Ruan, Y., Lin, H., Zhao, Z., Ku, J.P., Sun, H., Lam, P.K., 2019. Occurrence and distribution of per-and polyfluoroalkyl substances (pfass) in the seawater and sediment of the south china sea coastal region. Chemosphere 231, 468–477.

Wee, S.Y., Aris, A.Z., 2017. Endocrine disrupting compounds in drinking water supply system and human health risk implication. Environ. Int. 106, 207–233.

Wee, S.Y., Aris, A.Z., 2023. Revisiting the forever chemicals, pfoa and pfos exposure in drinking water. NPJ Clean Water 6, 57.

Weigend, F., Ahlrichs, R., 2005. Balanced basis sets of split valence, triple zeta valence and quadruple zeta valence quality for h to rn: Design and assessment of accuracy. Phys. Chem. Chem. Phys. 7, 3297–3305.

Yee, M.S.L., Hii, L.W., Looi, C.K., Lim, W.M., Wong, S.F., Kok, Y.Y., Tan, B.K., Wong, C.Y., Leong, C.O., 2021. Impact of microplastics and nanoplastics on human health. Nanomaterials 11 (496).

Zenobio, J.E., Salawu, O.A., Han, Z., Adeleye, A.S., 2022. Adsorption of per-and polyfluoroalkyl substances (pfas) to containers. J. Hazard. Mater. Adv. 7, 100130.